Journal of Structural Geology 31 (2009) 707–718

Contents lists available at ScienceDirect

Journal of Structural Geology

journal homepage: www.elsevier.com/locate/jsg

Aperture-size scaling variations in a low-strain opening-mode fracture set, Cozzette Sandstone, Colorado

J.N. Hooker*, J.F.W. Gale, L.A. Gomez [1], S.E. Laubach, R. Marrett, R.M. Reed

Bureau of Economic Geology, Jackson School of Geosciences, University Station, Box X, The University of Texas at Austin, Austin, TX 78713, USA

ARTICLE INFO

Article history:
Received 18 June 2008
Received in revised form
28 February 2009
Accepted 12 April 2009
Available online 18 April 2009

Keywords:
Fracture
Aperture size
Cozzette Sandstone
Power law

ABSTRACT

The aperture-size distribution of a set of opening-mode fractures in the Cozzette Sandstone is complex and cannot be described uniquely by a single equation. This study of horizontal core includes aperture-size data of macrofractures measured using a hand lens and microfractures measured using scanning electron microscope-based cathodoluminescence (SEM-CL). Macrofractures are poorly cemented, and total fracture strain is an order of magnitude lower than the smallest strain values of most previously described vein sets. Macrofractures in this set therefore resemble typical joints, as opposed to veins, in most respects. Although intragranular microfractures compose about 98% of the microfracture population, orientation, fracture fill, and fracture trace characteristics suggest that only transgranular microfractures can be shown to be genetically related to macrofractures. Aperture-size data below ~0.012 mm and above ~1 mm follow a log-normal distribution. Intermediate-size data, though relatively sparse, suggest a power-law aperture-size distribution. These results support the notion that this fracture set is an intermediate case between typical veins and joints. The results also suggest that processes leading to size distributions commonly associated with veins (i.e., power laws) may be present in joint sets, but over a more limited range, bound at small size-scales by grain-scale effects and above by mechanical layering effects.

1. Introduction

Size scaling of geologic fractures is a well-studied problem, primarily because of its potential to use populations of microfractures (fractures requiring a microscope to be detected), which can be sampled in core, to predict the abundance of macrofractures (fractures large enough to be identified by the naked eye—Laubach, 1997) in the subsurface. Opening-mode fractures commonly show size distributions that can be described using power laws (Gudmundsson, 1987; Barton and Zoback, 1992; Clark et al., 1995; Gross and Engelder, 1995; Loriga, 1999; Marrett et al., 1999; Ortega and Marrett, 2000; Gillespie et al., 2001; Laubach and Ward, 2006; Ortega et al., 2006), in which the number of fractures present in a population, of a given size or larger, varies with that size raised to some power. Sampling biases (Baecher and Lanney, 1978; Pickering et al., 1995) are often invoked to demonstrate an underlying power law when a lognormal or exponential best-fit trendline better fits size data collected (Bonnet et al., 2001). Fracture populations with power-law size distributions are said to be scale-invariant in that they lack a characteristic size scale; however, in reality, fracture-size power laws must be bracketed between the atomic scale and the scale of the Earth's crust, if not much more narrowly. The boundaries of power laws are not well understood and yet their delineation is critical to achieving an understanding of unsampleable subsurface fracture networks.

In addition to the problem of unknown power-law extent, most previous fracture size studies are based on vein sets with a wide range of sizes and, in typical cases, a nontrivial fracture strain (>0.025). Studies of fracture size distributions have historically used cement-filled fractures (called *veins*) because the cement fill in such fractures preserves the fractures' kinematic apertures (distance between original fracture walls, regardless of the presence or absence of cement—Marrett et al., 1999) and lengths, in outcrop and in thin section, making size easily measurable. In contrast, size distributions of poorly cemented opening-mode fractures, or *joints*, are poorly documented. A host of problems plague the measurement of joint sizes. Joint lengths are difficult to measure because joints are commonly longer than the outcrop that hosts them, so their true length cannot be measured. Branching trace patterns further complicate joint-length measurement. Joint apertures are difficult to study because they are generally too small

* Corresponding author. Tel.: +1 512 232 2254; fax: +1 512 471 0140.
E-mail address: john.hooker@beg.utexas.edu (J.N. Hooker).
[1] Present address: ExxonMobil Upstream Research Company, 3120 Buffalo Speedway, Houston, TX 77098, USA.

0191-8141/$ – see front matter © 2009 Elsevier Ltd. All rights reserved.
doi:10.1016/j.jsg.2009.04.001

to measure using a mm-scale ruler. Moreover, the poorly cemented nature of joint walls renders them susceptible, in outcrop, to erosive widening.

The few extant systematic studies of joint sizes have produced different conclusions as to their scaling properties: Odling (1997) documented a power-law joint-length distribution in Norwegian sandstones, but Gillespie et al. (2001) found a lognormal joint-length distribution in Irish limestones, in contrast to a power-law distribution of vein lengths in the same rock. This lack of a power law in joint sizes was hypothesized to be the result of fracture processes under low-differential stress near surface conditions, but there has been little systematic study of size scaling of opening-mode fractures at shallow depth. Consequently, size distributions are well studied in high fracture-strain vein sets, but the size distributions of low-strain, poorly mineralized fracture sets are not well understood, despite their common importance for subsurface fluid flow. Essentially all previous studies of joint size distributions have focused on length; joint aperture-size distributions remain unstudied.

This study presents fracture sizes in a horizontal core that was drilled perpendicular to a set of subsurface opening-mode fractures. Many fractures in the array are open, having only a thin veneer of quartz cement on fracture walls. In this respect these structures resemble joints. The fractures are the product of deformation at shallow crustal levels; the layer-parallel core segment's true vertical depth is approximately 2420 m and the host rocks have never been buried to depths of more than 4 km or to temperatures above 170 °C (Nuccio and Roberts, 2003). Fracture strain from the set examined here is about 0.0025—more than an order of magnitude lower than the smallest strain measured in previously studied vein sets.

Truly barren fracture walls are an unlikely result of fracture growth in diagenetically reactive subsurface environments, so the terms *vein* and *joint* are not helpful in most geologic fracture studies. The term *opening-mode fracture* lacks possibly misleading implications about fracture–cement content and best fits the structures studied here. The results presented here suggest that processes leading to scaling patterns recognized in veins also affect fracture growth in open fractures that in many respects resemble joints.

2. Geologic setting

In the southeastern Piceance basin, the dominant set of subsurface opening-mode fractures in the Mesaverde Group strike west-northwest (Lorenz and Finley, 1991). This fracture set was sampled by the N4°W-trending SHCT-1 well near Rifle, Colorado (Lorenz and Hill, 1991). This slant and horizontal well was drilled as part of a Department of Energy project to evaluate tight-gas sandstones in the Piceance basin (Fig. 1). At maximum deviation, including the interval used in the study, core was oriented at 85° from vertical, roughly parallel to the regional structural dip of 2° to 3° to the north-northeast.

The part of the core that we used is from the Upper Cretaceous Cozzette Sandstone Member of the Iles Formation (Mesaverde Group), from 2710 to 2776 m (8890–9108 ft) measured distance and about 2420 m true depth. The Mesaverde Group comprises marine/nonmarine deposits. The Cozzette Sandstone is a marginal marine sandstone, possibly shoreface or offshore-bar facies grading upward into barrier or strandplain facies (Zapp and Cobban, 1960; Quigley, 1965; Johnson and Keighin, 1981; Lorenz, 1983; Dutton et al., 1993). In this area the Cozzette is about 60 m thick. Most Cozzette sandstones are sublitharenites (Hansley and Johnson, 1980), but locally abundant mica grains and detrital dolomite qualify the sandstones as litharenites (Gomez et al., 2003). The

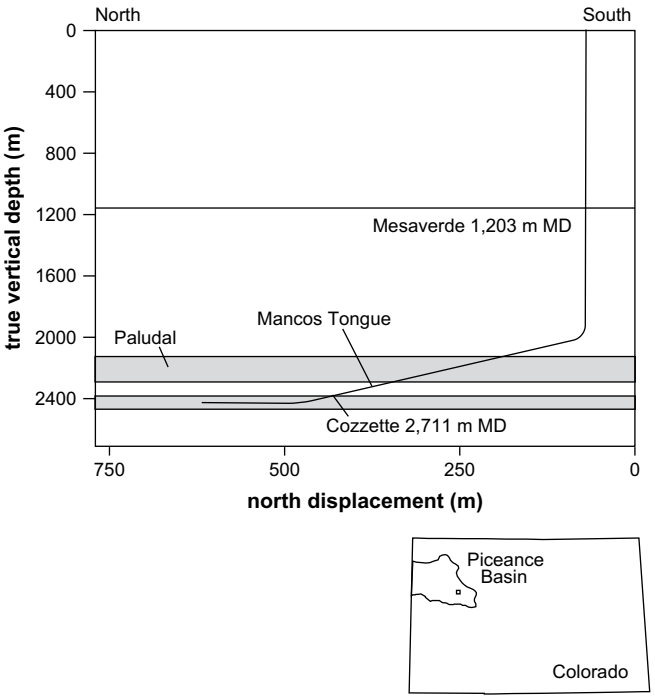

Fig. 1. Diagram of SHCT-1 core geographic and stratigraphic location. After Mann (1993).

cored interval is a fine- to medium-grained sandstone. Grains are angular, and detrital silt is present (~5%). The primary cement is quartz (~12%); clay and carbonate minerals are also present but volumetrically insignificant (<5%).

Vitrinite reflectance (Nuccio and Roberts, 2003) demonstrates that nearby rocks at the base of the Mesaverde Group achieved a maximum burial temperature of approximately 170°C, corresponding to a burial depth of about 4000 m. Burial history reconstructions (Nuccio and Condon, 1996; Nuccio and Roberts, 2003) based on various constraints indicate that this maximum burial was reached near 35 Ma; uplift began near 10 Ma, bringing the rocks studied to their present burial depth.

Opening-mode fractures at depth in a sedimentary basin having near-horizontal beds may develop when pore-fluid pressure and minimum principal horizontal stress combine to produce a positive driving stress for crack propagation (Secor, 1965; Segall, 1984). Lorenz and Finley (1991) interpreted fracture propagation of these west-northwest-striking fractures to reflect regional maximum horizontal stress (S_{hmax}) during the Late Cretaceous, with fracture development possibly enhanced by subtle local folding.

3. Methodology

3.1. Calculating fracture intensity in one and two dimensions

Fracture *intensity* is a size-specific quantification of fracture abundance (Ortega et al., 2006). Because the macrofractures sampled cut the core at right angles to its length (Fig. 2), the core approximates a one-dimensional line of fracture observation, or *scanline* (Fig. 3). In the case of a single set of parallel, opening-mode fractures, fracture intensity is calculated by measuring the kinematic aperture of each fracture along a scanline and plotting these aperture sizes versus cumulative frequency. Cumulative frequency is cumulative number (1 for the largest fracture, 2 for the second-largest, and so on) divided by scanline length. Fracture intensity may also be calculated in 2d fracture maps, in which case frequency

Fig. 2. Segment of SHCT-1 layer-parallel core, measured depth 9037 ft, used for SEM-CL microfracture analysis. Core diameter is 67 mm. Face is horizontal, view from the top. Approximate areas sampled by contiguous thin sections (A–H) shown. Broken surface consisting of one wall of a natural macrofracture is circled.

of fractures per unit area is calculated instead of per unit length. Fracture intensity can be calculated using either length or aperture, but measuring fracture length in a horizontal core is impossible for most macrofractures. This study therefore focuses on macro- and microfracture aperture.

3.2. Sampling

Microfracture apertures measured along scanlines are analogous to macrofracture apertures measured in horizontal core and provide the opportunity to compare fracture intensities at different scales. Two-dimensional microfracture maps were also analyzed in this study for two reasons in order to analyze microfracture strike, and to take full advantage of the high number of microfractures sampled, compared to macrofractures.

Eight samples from the SHCT-1 core were taken for scanning-electron-microscope-cathodoluminescence (SEM-CL) analysis. Six of these samples were individual thin sections, analyzed in 1d (Fig. 4). The remaining two samples were approximately 28-cm-long segments, from measured depths of 9037 ft and 9062 ft. These larger samples were analyzed in 1d and in 2d. The objective in selecting core segments was to analyze long, intact samples, so that a large population of *micro*fractures (fractures requiring a microscope to be detected) could be sampled and uncertainties related to reassembling broken parts could be avoided. Distance from macrofractures was not considered during sample selection, though it may play a role in microfracture organization.

Scanline 9037 intersects only one macrofracture, half of which is preserved (Fig. 2). Scanline 9062 intersects two macrofractures

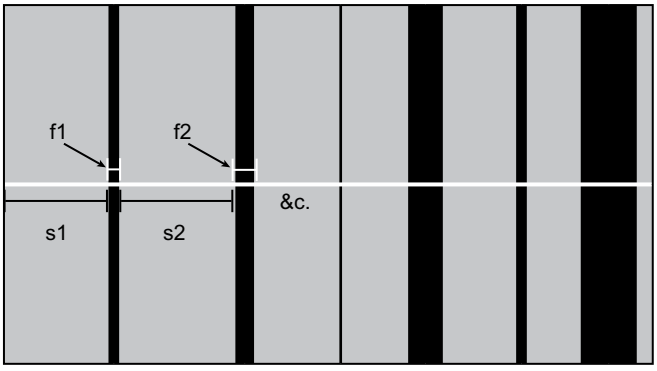

Fig. 3. Fractures measured along a 1d scanline. Idealized fractures are black; host rock is gray. The scanline (white) is drawn over a surface containing fracture traces (such as an SEM-CL image), perpendicular to the dominant fracture trend. Fracture kinematic apertures (f1, f2) are measured as the distance along the scanline within fracture walls. Spacings (s1, s2), which were not analyzed in this study, are measured as the distances along the scanline between fractures. The total scanline length is the sum of all spacings and fracture apertures.

(Fig. 4). To analyze the core segments, a horizontal face of the core was slabbed at a width of less than 25 mm so as to fit within 25 × 46-mm (1 × 2-inch) layer-parallel thin sections. The slab was then deliberately broken at intervals of less than 46 mm so as to make each thin section contiguous with the next, with no loss of rock between adjacent sections (Gomez and Laubach, 2006) (Fig. 2). This method allowed the collection of a complete inventory of microfractures in each multi-thin-section-long segment.

3.3. SEM-CL imaging

Samples were imaged using an Oxford Instruments MonoCL2 cathodoluminescence detector system, attached to a FEI XL30 scanning electron microscope (SEM) operating at 15 kV with a large spot size. At 150×, a single SEM-CL image has an area of only 0.45 mm^2 and is 0.77 mm wide, so the entire length of contiguous thin-section sets was imaged using an overlapping mosaic method. The configuration of the CL mirror prohibited lower magnification. Fractures were digitized, in two dimensions and along digitally-overlain scanlines, on the SEM-CL imagery. Microfracture apertures and orientations were digitized by hand, classified, and electronically calculated, facilitating systematic collection of large microfracture datasets (Gomez and Laubach, 2006). One pixel in SEM-CL images is 0.00076 mm wide.

The Cozzette Sandstone presents several challenges to SEM-CL imaging and microfracture analysis. Under electron bombardment, quartz luminesces much more faintly than most feldspars and carbonate minerals. Because of this contrast it is far more challenging to image polymineralic siliciclastics such as the Cozzette Sandstone than, for example, a quartzarenite (Reed and Milliken, 2003). In addition, in the absence of pervasive quartz cement, grain-scale fractures tend to circumnavigate grains while propagating, seeking out weaker interfaces along which to propagate. Finally, fracture strain in the Cozzette Sandstone is relatively low. For these reasons, this study represents a more rigorous test of our methodology than does a study of a high-fracture-intensity quartzite (e.g., Laubach and Diaz-Tushman, 2009). If quantitative characterization of a microfracture set using SEM-CL is possible in the Cozzette Sandstone, then it is possible in a wide variety of sandstones.

4. Fracture description

4.1. Macrofracture attributes

SHCT-1 core in the Cozzette Sandstone, which is about 35 m long, contains 26 subvertical, opening-mode fractures. Macrofractures dip steeply, are perpendicular to gently (2–3°) dipping beds, and have a consistent west-northwest strike and a narrow strike range (Fig. 5). Most have sharp, straight traces, although on the microscopic-scale fracture walls they frequently deviate around

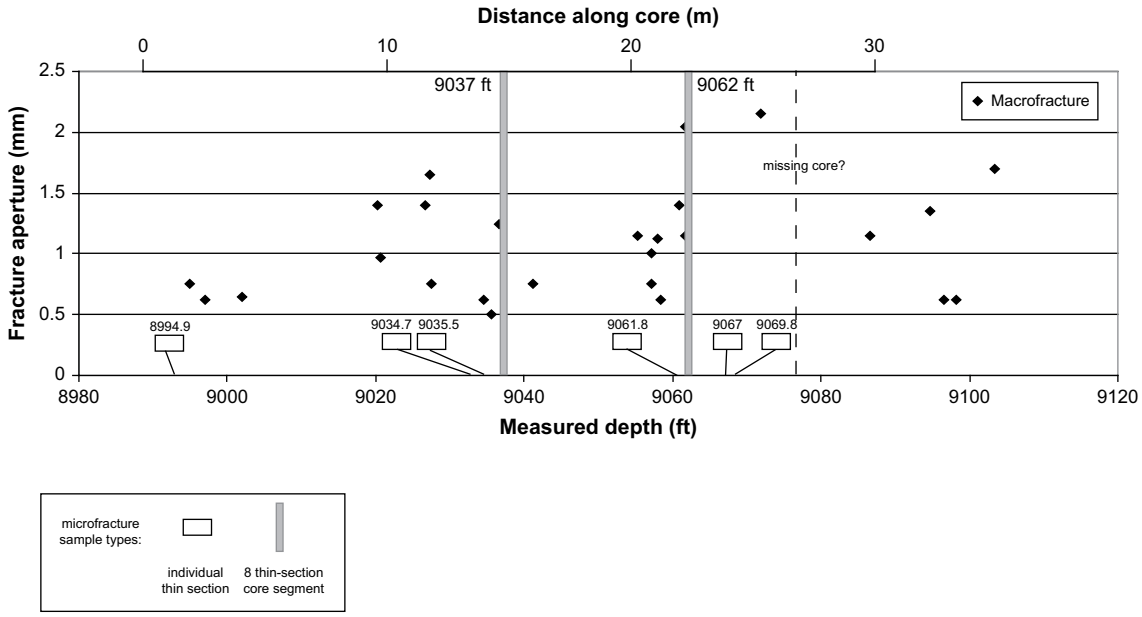

Fig. 4. Plot of macrofracture aperture versus position in SHCT-1 horizontal core. Microfracture sample locations shown (rectangles not to scale). After Lorenz and Hill (1991) and Gomez et al. (2003).

grains, imparting a submillimeter rugosity. Observations of offset grains on opposite fracture walls show that these are opening-mode fractures.

The 26 macrofractures are porous and lined but only locally filled with quartz cement. They also locally have traces of calcite cement. On open fractures, the veneer of quartz cement is typically only a few tens of microns thick and, thus, inconspicuous unless observed using high magnification. Where macrofractures are intact but not entirely filled with cement, quartz tends to form isolated deposits that bridge fracture walls. Where calcite is present, overlap relations suggest that it postdates quartz.

4.2. Microfracture attributes

The vast majority of fractures sampled are intragranular, meaning that both fracture tips lie within a single detrital grain (Laubach, 1997). One hundred and ninety-seven transgranular microfractures were measured in 299 mm^2 (a fracture density of 0.66 fractures per mm^2); 4697 intragranular microfractures were measured in 106 mm^2 (a fracture density of 44 fractures per mm^2). Scanline 9037 intersects 879 fractures (Fig. 6A), 7 of which were interpreted as transgranular. Scanline 9062 intersects 790 total microfractures, 7 of which were interpreted as transgranular. Microfracture scanlines from the six individual thin sections analyzed range in length from 5.2 to 29.3 mm (Fig. 6B). The number of transgranular microfractures encountered, normalized per meter, ranges from 0 to 385. The total number of microfractures encountered ranges from 1546 to 2697 per meter.

Some transgranular fractures crosscut multiple grains and have consistent strikes and sharp boundaries throughout their lengths, resembling macrofractures in orientation, crosscutting relations, and internal texture. An example is shown in Fig. 7; the large microfracture is primarily quartz filled but locally contains calcite cement and porosity.(Fractures narrower than the fracture shown, i.e. those with <0.1 mm aperture, rarely preserve any porosity. We therefore estimate the *emergent threshold* (Laubach, 2003) of Cozzette Sandstone fractures to be 0.1 mm.) The fracture trace is generally straight but locally deflects at grain boundaries. In general transgranular microfractures strike parallel to macrofractures

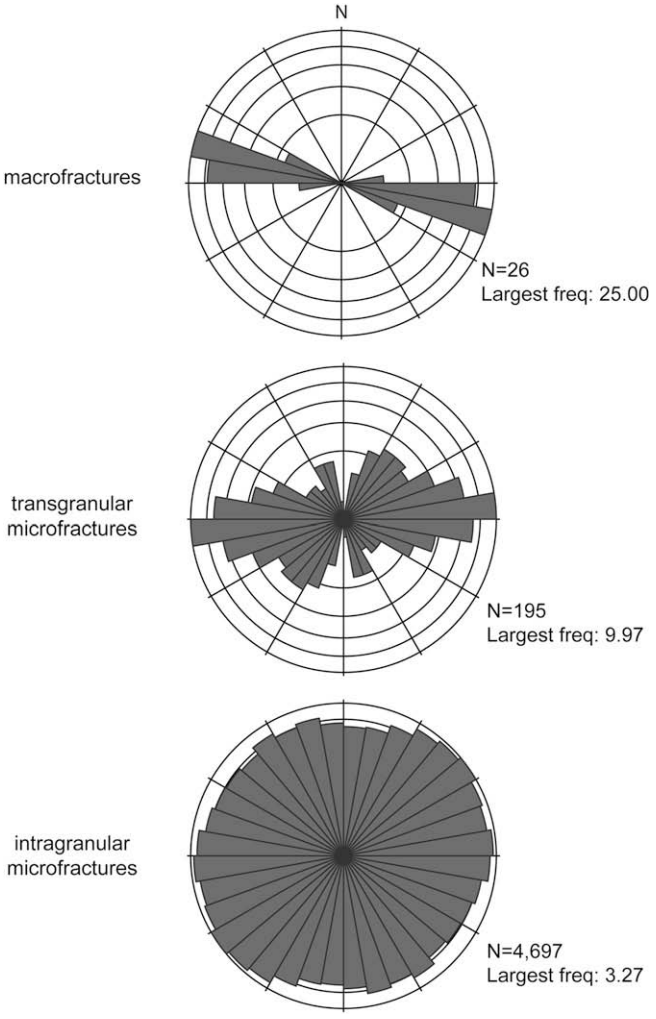

Fig. 5. Rose diagrams of fractures from SHCT-1 core. Transgranular microfractures were measured from maps from samples 9037 and 9062. Intragranular fractures were measured from sample 9037.

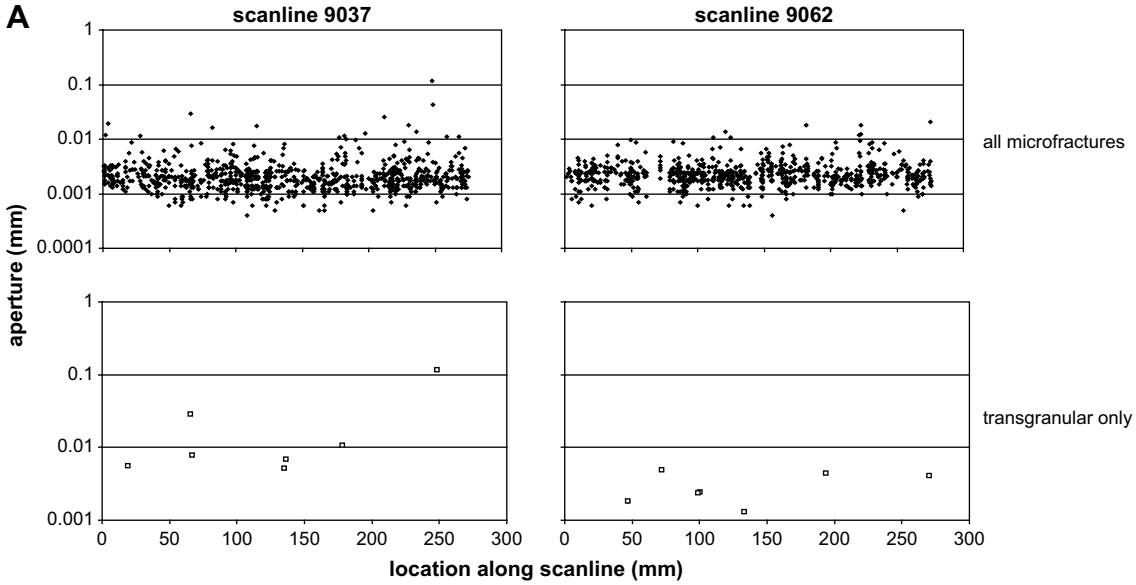

879 3182.5	total fractures per meter	789 2842.2
7 25.3	transgranular microfractures per meter	7 25.2

Fig. 6. Plots of microfracture aperture vs. location along scanline. (A) Multiple thin section scanlines.(B) Single thin section scanlines.

(Fig. 5); transgranular microfractures and macrofractures also have similar crosscutting relationships and internal textures (cement, porosity).

Intragranular microfractures display a wide range in strike, in contrast to the orientations of transgranular microfractures and macrofractures (Fig. 5). Most intragranular microfractures are sealed. Many intragranular fractures are straight and have sharp, distinct boundaries. Others have curved walls and indistinct, gradational boundaries that have been interpreted to reflect crystallization processes of plutonic quartz (Sprunt and Nur, 1979; Seyedolali et al., 1997; Bernet and Bassett, 2005) or dissolution/precipitation in hydrothermal vein quartz (Rusk and Reed, 2002; Landtwing and Pettke, 2005). Similar textures are occasionally present in transgranular microfractures (Fig. 8).

Many microfractures are present in the dataset that may be transgranular but were not counted as such. This is the case when either the fractures do not cut cement in between the grains they cross (such fractures cut touching grains and may have been formed during early compaction) or the fracture–cement relationship is unclear because of low contrast in cement patterns or plucking during thin-section polishing. In either case, what appears to be a single transgranular microfracture may really be two intragranular microfractures, aligned by chance. Such fractures were not included in those analyses based only on transgranular microfractures.

Microfractures specifically attributable to grain crushing during compaction were ignored in this study. Such fractures have patterns, shapes, and timings that indicate that they formed as the result of neighboring grain interactions and not regional stress (Dickinson and Milliken, 1995). Evidence includes wedge shapes, fracture orientation with respect to grain contacts, and patterns that resemble grain-scale breccia networks (Fig. 9A). These fractures typically affect single grains or pairs of grains in contact. In addition, microfractures specifically attributable to inheritance from previous source rocks were also ignored; such fractures were identified by wide apertures truncated at grain boundaries (Fig. 9B). Timing constraint of intragranular fractures not specifically attributable to grain crushing or inheritance is difficult; these fractures were therefore dealt with separately in the analysis (see below).

5. Aperture-size distributions

5.1. Macrofracture size distribution

We obtained aperture measurements of 26 macrofractures. The kinematic aperture of the narrowest macrofracture is 0.5 mm; the widest is 2.15 mm. Truncation effects (Baecher and Lanney, 1978) on macrofracture sampling should be negligible because the smallest aperture is plainly visible under a 10 × hand lens. Smaller-aperture fractures are difficult to detect, however, because as fracture offset approaches grain size (0.1–0.5 mm), the fracture trace becomes indistinguishable from grain boundaries; fracture cement is indistinguishable from matrix cement.

The SHCT-1 core is broken along 20 of the 26 macrofractures, occurring along open and mostly open fractures during core recovery and handling. Estimates of fracture aperture of these broken fractures were made by measuring the height of crystal linings on fracture walls, providing minimum estimates of true fracture width. The absence of borehole breakouts suggests fractures wider than a few mm are not present where drilling occurred.

The aperture-size distribution of macrofractures measured in core is shown in Fig. 10. The data show a broad, concave-down curve. This curve was fit with normal, log-normal, power law, exponential, and logarithmic trendlines, for which R^2 values were compared to determine the best fit. Of the five trendline types, logarithmic had the highest R^2 value (Table 1), indicating the best fit, although all trendlines *except* power law give R^2 values >0.95. This macrofracture aperture-size distribution is not adequately describable using a power law, either because the fractures do follow a power law in reality and uncertainties in aperture measurements and unknown censoring effects biased our data, or because a real deviation from a power law in the fracture-size pattern exists.

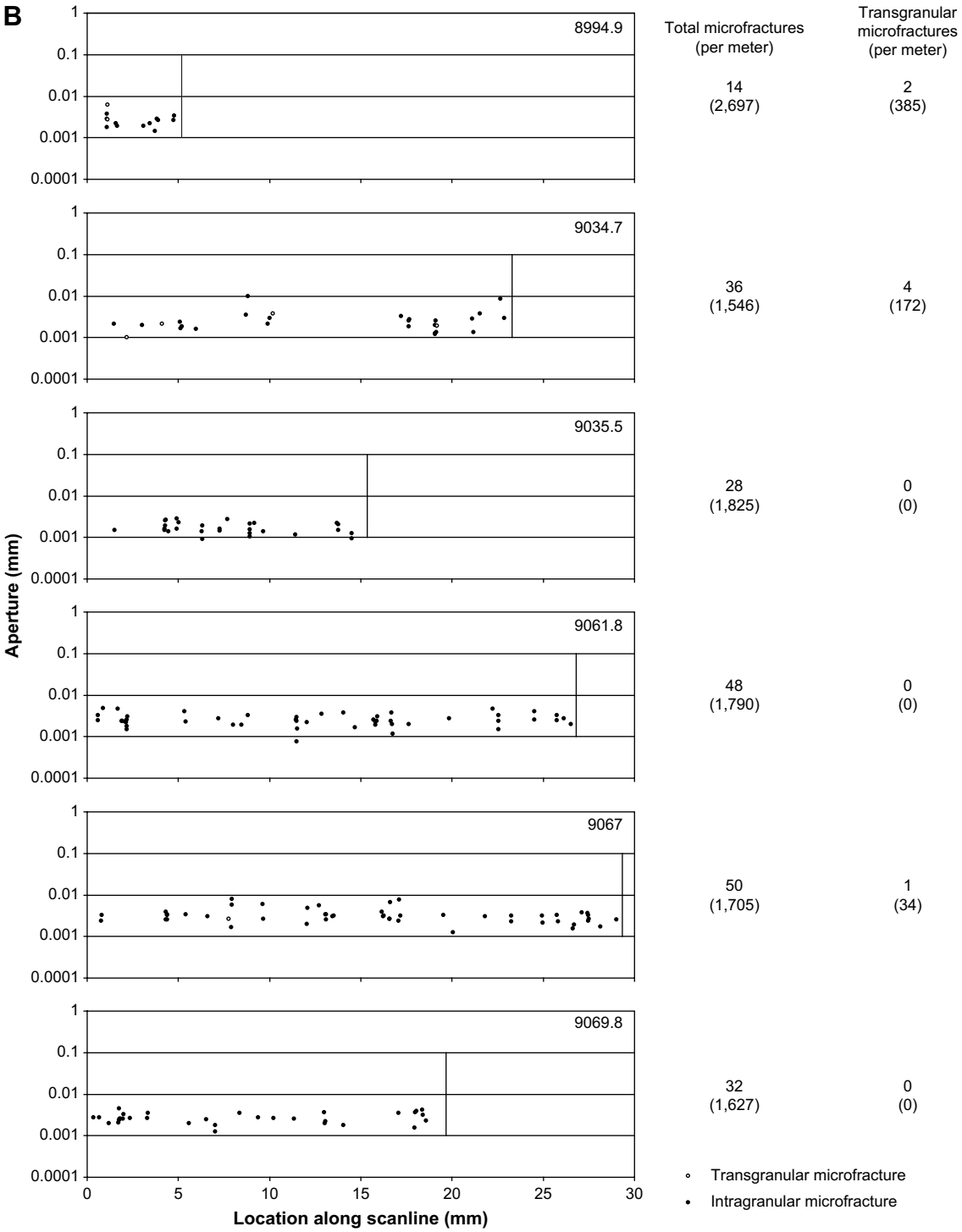

Fig. 6. (*continued*).

5.2. Microfracture size distributions

Microfractures measured in 2d range in aperture from 0.00056 to 1.2 mm. Transgranular microfractures range in aperture from 0.001 to 1.2 mm. Fig. 11 shows cumulative frequency–aperture data for transgranular and intragranular microfractures.

The cumulative frequency–aperture data curves for all transgranular and intragranular microfractures measured in 2d were fit with the same trendline types fit to the macrofracture size distribution to determine the best equation for microfracture-size distributions. As with the macrofracture data, R^2 values were compared between best fits. In all three cases, the highest R^2 value is that for a log-normal distribution.

Because microfracture intensity measured along a scanline is analogous to the way macrofractures were sampled and measured, the intensity of the two 1-dimensional datasets can be compared. In all, 1877 microfractures were measured along one-dimensional scanlines totaling 625 mm in length; these microfractures range in

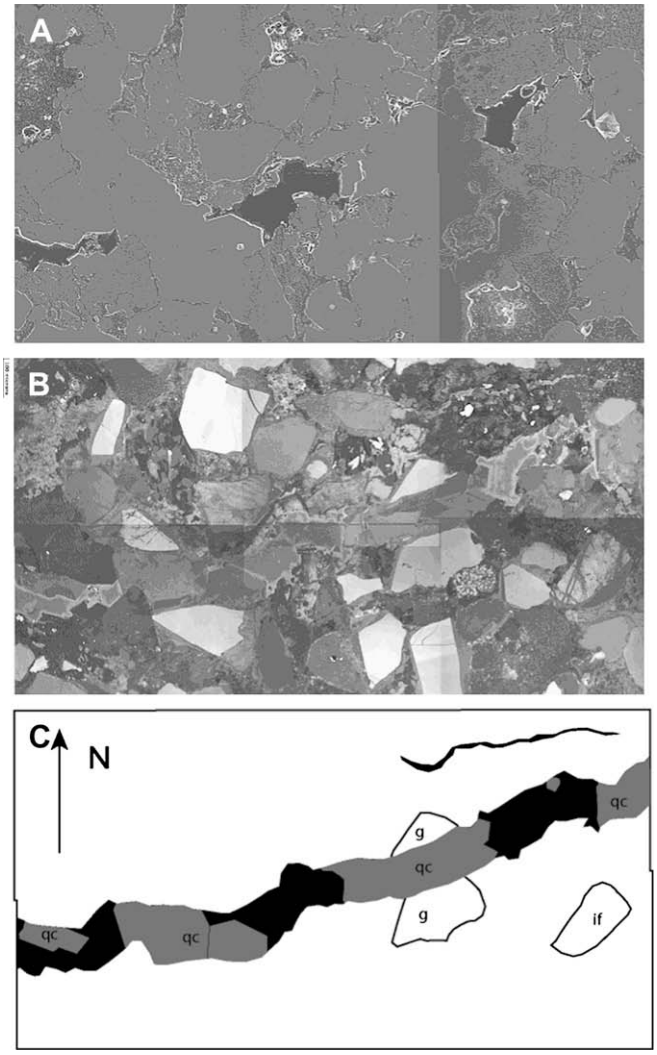

Fig. 7. Transgranular microfracture, revealed by SEM-CL.(A) Secondary electron image showing relief of the thin section. Porosity is darker than surrounding area. Note that porosity is primarily fracture related.(B) Panchromatic grayscale SEM-CL image. Quartz grains are white to medium gray; lithic fragments show various multishaded patterns.(C) Interpretation. Fracture porosity is in black, with synkinematic quartz cement (qc) in dark-gray (note zoning in B). A quartz grain (g) has been displaced by the fracture. A small fracture, which also preserves porosity, is shown at top right. Another quartz grain features abundant microfractures inherited from previous source rock (if), as evidenced by the truncation of its fractures at the grain boundary.

aperture from 0.0009 to 0.116 mm. The 28 transgranular microfractures measured along scanlines range in aperture from 0.001 to 0.116 mm. Cumulative frequency–aperture data curves for fractures measured along scanlines are qualitatively similar to those curves for the two-dimensional fracture map (Fig. 12).

6. Discussion

6.1. Interpretation of microfracture genesis

Images acquired from SEM-CL plainly document microfractures in the Cozzette Sandstone. Because of similar orientation, trace characteristics, and fracture–cement relationships between transgranular microfractures and macrofractures, these microfractures are most simply interpreted as smaller members of the same fracture set, which also includes macrofractures.

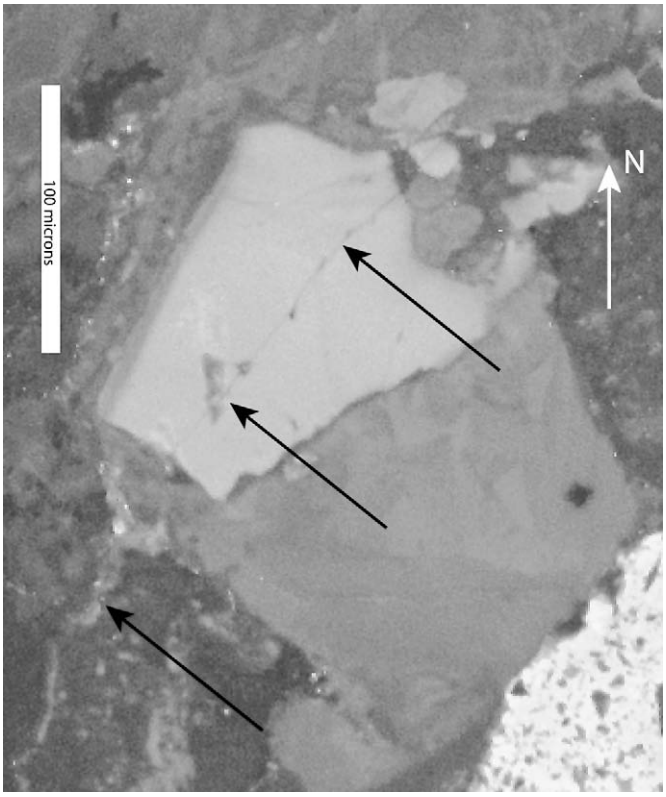

Fig. 8. Transgranular microfracture. Note patchy fracture trace and abnormal strike.

The Cozzette Sandstone, along with other foreland-basin sandstones in the western United States, contains a rich array of inherited intragranular quartz-filled microfractures in detrital quartz grains. These are useful as provenance indicators (Seyedolali et al., 1997; Bernet and Bassett, 2005; Hooker and Laubach, 2007) but impede interpretation of small microfractures that formed in situ. The wider scatter of strikes of intragranular fractures suggests that not all of these are small versions of the regional tectonic fractures represented by transgranular fractures and macrofractures, therefore their size populations are analyzed separately. Intragranular microfracture do not have the same characteristics (trace, orientation) of macrofractures, and therefore are not interpreted to be members of the same fracture set.

6.2. Interpretation of microfracture intensity curves

Previous work (Gomez et al., 2003) described microfractures measured from the same core as following a power law size distribution. Concave-down fracture intensity curves have commonly been interpreted as power law size distributions affected by sampling biases (Bonnet et al., 2001). One interpretation of the aperture-size distribution of the intragranular microfractures is that they form a power law with an exponent of approximately −3.3 (Fig. 13A). If this power law is real and persists at the subgranular scale, then the rollover in the aperture-size distribution below 0.0025 mm is best explained as a truncation bias, i.e., that the rollover is present because the smallest fractures were missed during fracture measurement. This interpretation is unsatisfactory because while microfractures of aperture >0.001 mm (1.3 pixels) are readily detectable using the imaging resolution applied in this study (4708 were measured in fracture maps), this power law suggests that more than 50,000 such microfractures should have

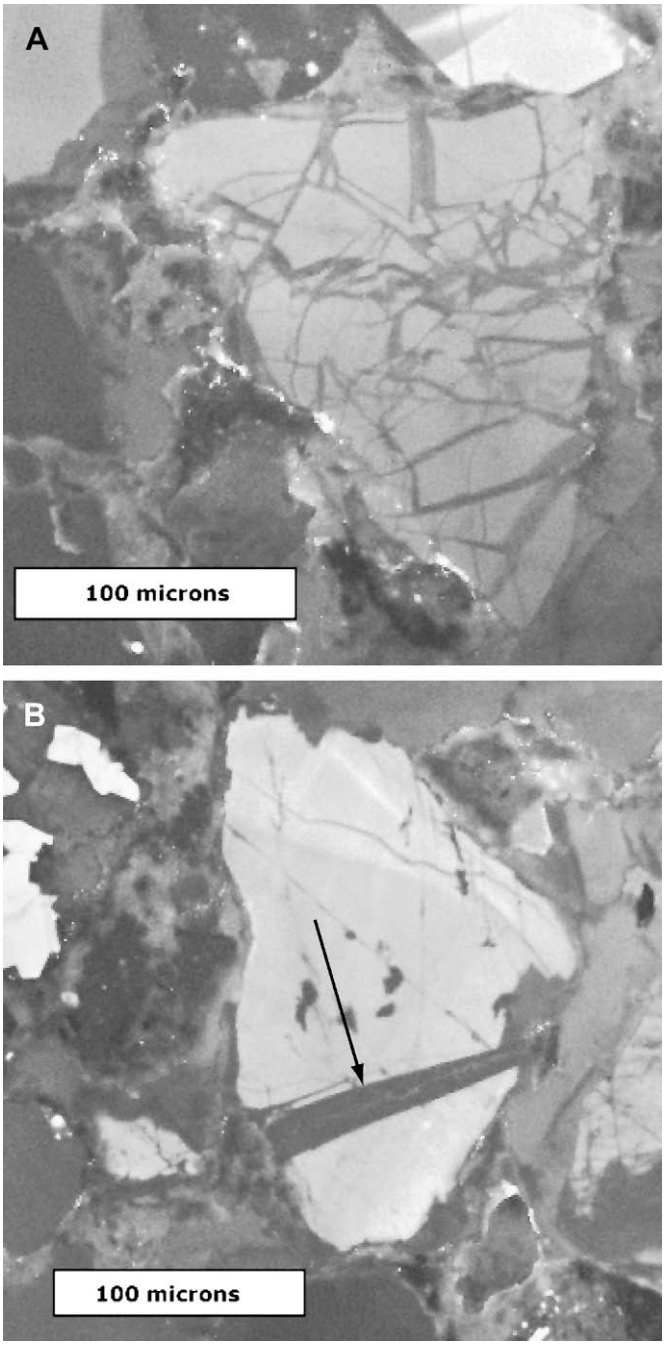

Fig. 9. Microfractures related to individual-grain crushing (A) were ignored in this study, as were fractures independently attributable to inheritance from previous host rocks (B—fractures that were already in the grain at deposition). See text for details on how these fractures were identified.

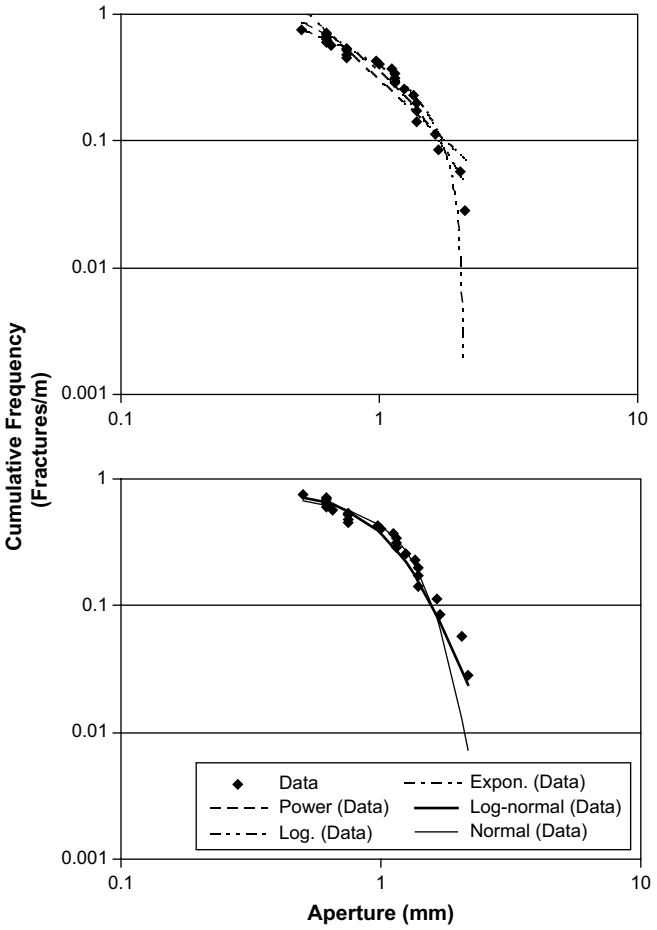

Fig. 10. Macrofracture aperture-size distribution. A log-normal curve best fits the distribution over normal, exponential, logarithmic, and power law (Table 1).

been detected. Therefore, if a power law is present among the intragranular microfractures, it appears to end, in reality, among fractures smaller than ~0.002 mm in aperture.

The majority of transgranular microfractures also closely follow a log-normal distribution (Fig. 11, Table 1). As is the case with the intragranular fracture aperture-size distribution, this result can be interpreted as a power law with sampling biases resulting in a concave-down curve to the data. This interpretation, for most of the transgranular microfractures, is inappropriate, but not for the difficulty in interpreting a truncation rollover discussed above for the intragranular microfractures. The interpreted underlying power law for transgranular microfractures would be much shallower, with an exponent near −1.4 (Fig. 13B). The number of fractures >0.001 mm wide that should have been present is therefore ~560, which is well below the density of intragranular fractures of that size. Therefore it is entirely possible that the missing fractures were not truly missed but binned with the intragranular microfractures, even though they formed along with the throughgoing fracture set.

However, the larger-aperture end of the aperture-size distribution cannot be explained by simple censoring biases (e.g., the maximum fracture length measurable in a finite-area fracture map). In such a case a concave-down curve would be apparent in the large-size end of the data, which curve may be interpreted in the aperture range near 0.007 to 0.012 mm, depending on where the power law segment is interpreted. The data from the largest fractures sampled (>0.012 mm) deflect *upwards* from this trend, indicating a complicated aperture-size distribution. Although a log-normal distribution curve fits this data with low statistical error, it does not account for this upswing in the aperture-size data of the largest fractures.

Another interpretation of the data is that the transgranular microfractures measured in 2d represent a transition from a log-normal size distribution, among the small microfractures, to a power law among the large microfractures (Fig. 13C). A log-normal trendline fits the fractures with apertures less than

Table 1
R-squared values for different fracture datasets.

Trendline type					
Dataset	Normal	Log-normal	Power law	Exponential	Logarithmic
2d					
Transgranular	0.167	**0.981**	0.879	0.120	0.664
Intragranular	0.909	**0.991**	0.348	0.907	0.866
1d					
Microfracture scanlines	0.576	**0.967**	0.914	0.574	0.861
Macrofractures	0.956	0.962	0.897	0.960	**0.969**

Best fits are given in bold.

0.012 mm ($R^2 = 0.996$). Not enough fractures were sampled to independently demonstrate a power law among the microfractures wider than 0.012 mm, but if a power law does exist, then a power-law extrapolation from such fractures, measured in 1d (matching the topology of the 1d macrofracture sampling), should coincide closely with the macrofracture aperture-size distribution. The aperture-size data trend of the transgranular microfractures intersected by scanlines in all thin sections made from the SHCT core (Fig. 12) is qualitatively similar to that of the 2d transgranular microfracture data. Extrapolation of a power law fit only to all transgranular microfractures wider than 0.012 mm (Fig. 14) predicts an abundance of 0.5 mm-wide or larger fractures of 0.622 fractures per meter, compared to an observed abundance of 0.743 (an under-prediction by a factor of 0.2). The extrapolation predicts an abundance of 1 mm-wide or larger fractures of 0.405 fractures per meter (an over-prediction by a factor of 0.01). Therefore, if a power-law aperture-size distribution persists between the observed scales, then the extrapolation from the transgranular microfractures reasonably approximates it.

The size range over which a power law likely exists contains little data. This is because fractures of such aperture sizes (between 0.01 and 1 mm) require SEM microscopy to be detected, and yet their average spacings are greater than the areas imaged using SEM-CL. Therefore they lie between the ranges thoroughly sampled in this study. This highlights the need for long scanlines or large fracture maps to adequately sample microfractures that reliably scale to macrofractures.

6.3. Implications

If present, a power-law aperture-size distribution among post-depositional fractures would be bracketed at lower ($<\sim$0.01 mm) and upper ($>\sim$1 mm) size limits. Below the lower limit, fractures follow a log-normal distribution. Although the smaller transgranular microfractures measured in this study are evidently genetically related to the larger ones, they follow a different type of size distribution. Fractures nucleate from flaws within rocks (Griffith, 1920) whose sizes are likely related to grain size in sandstone. It is apparent in this study that some flaw-fracture propagation took place before a power law was established, suggesting that some process like fracture linkage or coalescence may be responsible for generating the power-law size distribution.

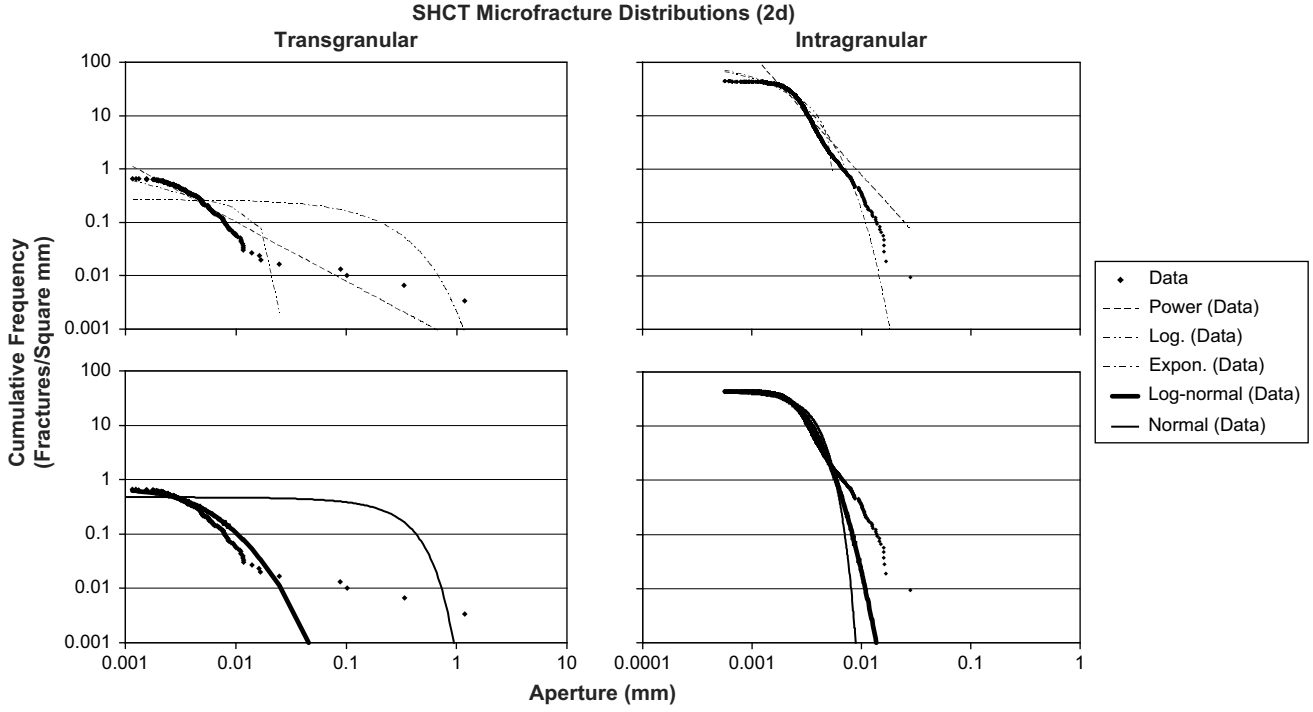

Fig. 11. Aperture-size distributions for transgranular and intragranular microfracture populations measured in 2d. Log-normal curves fit the plots with the lowest statistical error, but visual inspection suggests the real size distribution is more complicated than any single equation.

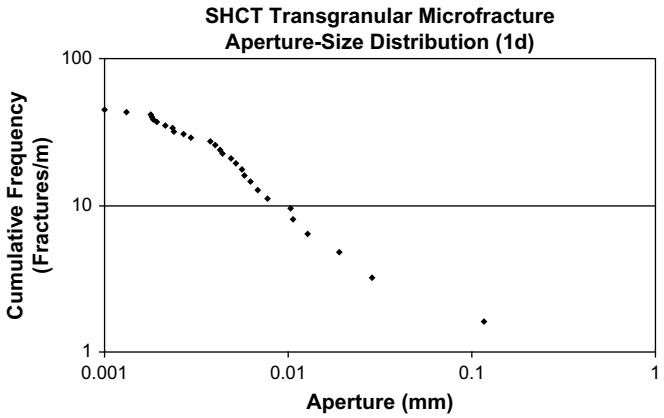

Fig. 12. Aperture-size distribution for all transgranular microfractures measured along scanlines. These fractures were measured in a way analogous to the measurement of macrofractures (Fig. 3) and therefore can be compared directly to the aperture-size distribution of macrofractures.

The fracture set studied is one of relatively low strain, as discussed above. Assuming that fracture sets progressively accommodate strain over time (i.e., that high-strain fracture sets initially resembled the Cozzette Sandstone fracture set in terms of amount of strain and fracture-size distribution), then the aperture-size distribution shown here suggests that power laws may develop early in the evolution of a fracture set. The interpreted power law in this study extends over a limited range; if these data represent an early stage in the evolution of a fracture set, this range may also grow with further fracture strain.

Just as the power law likely does not extend to sub-granular scales, it cannot extend to infinitely large scales, either. Extrapolation of the power law derived from transgranular microfractures towards larger fracture sizes indicates that one should expect a fracture more than 30 km wide within the ~110 km-wide Piceance basin, which fracture size is almost certainly not present. The concave-down curve of the macrofracture data may indicate where the interpreted power law stops, in reality. Gillespie et al. (2001) ascribed the lack of scale invariance in joint sizes to suppression of crack propagation (and crack-tip stress intensity) for joints formed under low-differential stress near surface conditions in mechanically layered rock. As a joint population grows, fracture density in a mechanical layer increases until no more joints can develop owing to the interaction of stress shadows, at which point the system is said to be *saturated* for the given stress conditions (Rives et al., 1992; Bai and Pollard, 2000). Gillespie et al. (2001) contrasted this style of joint-set evolution with vein-set growth, which occurs at a depth sufficient to strengthen rock-layer boundaries so that they will not slide to accommodate fracture opening (Renshaw and Pollard, 1995). A propagating vein will thus cut across bedding planes, becoming longer and achieving higher and higher crack-tip stress intensity. Resulting faster growth of larger fractures hypothetically fuels power-law size distributions. Numerous studies of *stratabound* versus *non-stratabound* fracture systems that document the apparent interference of mechanical layering on power-law fracture-size development are summarized in Odling et al. (1999).

The fractures documented in this study share attributes common to veins and joints. If a critical factor in determining which type of fracture will develop is the presence of mechanically significant layering, then the relatively low maximum burial depth of the Cozzette Sandstone may well explain the jointlike nature of macrofractures: the rocks were sufficiently

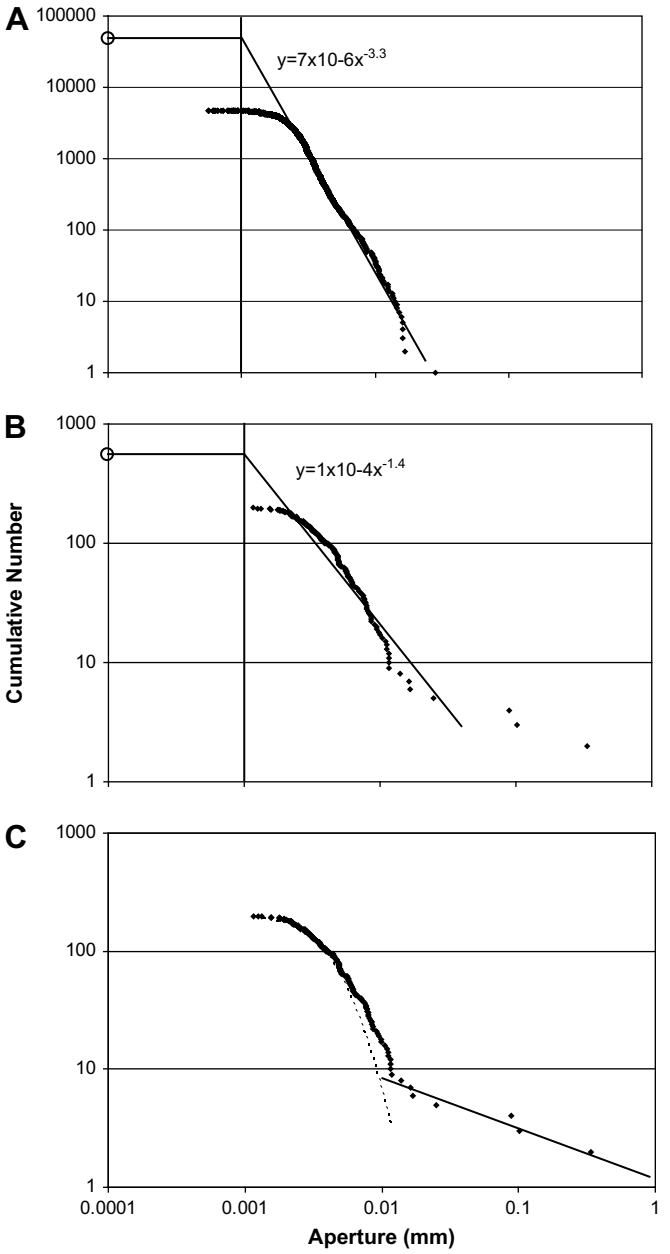

Fig. 13. (A) Power law fit to the intragranular microfracture size distribution (2d), accounting for a possible truncation bias of the smallest fractures. Truncation bias is likely not the sole reason for the rollover in (A), as it suggests more than 45,000 fractures should be present between 0.001 and 0.002 mm.(B) Transgranular microfracture distribution (2d). A truncation bias is more plausible for the transgranular microfracture rollover, but a power law (straight-line) segment is not likely present; the aperture-size distribution swings down and then up again at larger sizes, suggesting a power law is not present at all scales.(C) Fit of log-normal distribution to fractures <0.012 mm wide and power law fit to larger fractures.

shallow for bedding-plane sliding, which may halt fracture propagation (Renshaw and Pollard, 1995). However, it is when growing fractures *reach* mechanical layering boundaries that their growth is arrested; before that, propagation in an isotropic medium should be assumed. Therefore, small fractures in a growing joint set may form power-law size patterns like those normally associated with veins because, like veins, they are not affected by mechanical layering. A parallel result was found for bedding-bound and non-bedding-bound fracture spacings by Gross and Engelder (1995).

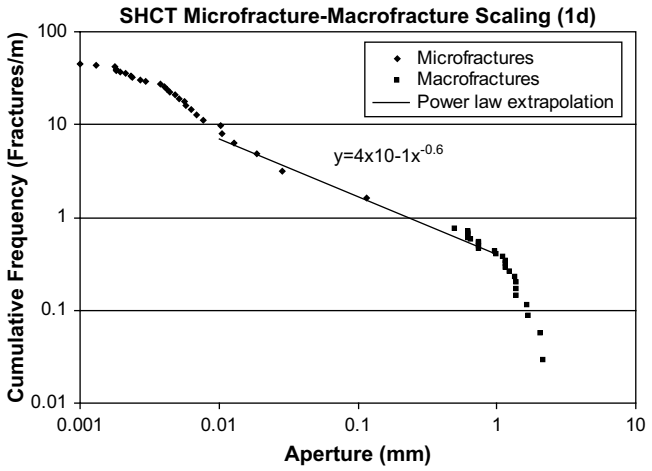

Fig. 14. Extrapolation of a power law from the largest microfractures measured in 1d towards larger fracture sizes. Note close fit to smallest macrofractures.

7. Conclusions

A set of shallow, low-strain, joint-like fractures in the Cozzette Sandstone follows an irregular aperture-size distribution. The smallest fractures ($<\sim$0.012 mm wide) and largest fractures ($\geq$0.5 mm wide) are best characterized by a log-normal distribution. Although limited intermediate-sized fracture data was measured, a power law fits the data present and connects the two better-observed scales with low statistical error. The smallest fractures appear to have propagated little beyond the granular scale; if power laws emerge from interaction among growing fractures, these small fractures may be too small to have been incorporated into such a system yet. Propagation interference by mechanical bedding boundaries may end the power law at the large-size end.

The fracture set is composed of microfractures that are sealed with quartz and large fractures that are mostly open. Because these large fractures are lined with only a thin veneer of quartz and/or calcite, they resemble joints. Because the Cozzette Sandstone fracture set shows degrees of cementation that vary with fracture aperture, the difference between open fractures or joints and filled fractures or veins is, in this case, a matter of size.

To reliably measure scaling using microfractures in these low-strain rocks, large image areas are essential. Large sample size permits an analysis based on large, transgranular microfractures that formed in situ. The vast majority of small microfractures are unrelated to the macrofracture set. Most of these fractures were inherited from source rocks of the grains and introduced into the rock at deposition.

Acknowledgments

Our research is supported by Chemical Sciences, Geosciences and Biosciences Division, Office of Basic Energy Sciences, Office of Science, U.S. Department of Energy Grant DE-FG02-03ER15430 and by industrial associates of the Fracture Research and Application Consortium. We are grateful for Lana Dieterich's editing, and for illuminating reviews by Noelle Odling, Charlie Onasch, and Joao Hippertt. This paper was published with permission from the Director of the Bureau of Economic Geology.

References

Baecher, G.B., Lanney, N.A., 1978. Trace length biases in joint surveys. In: 19th U.S. Symposium on Rock Mechanics, University of Nevada, Reno, pp. 56-65.

Bai, T., Pollard, D.D., 2000. Fracture spacing in layered rocks: a new explanation based on the stress transition. Journal of Structural Geology 22, 43–57.

Barton, C.A., Zoback, M.D., 1992. Self-similar distribution of macroscopic fractures at depth in crystalline rock in the Cajon Pass scientific drill hole. Journal of Geophysical Research 97 (B4), 5181–5200.

Bernet, M., Bassett, K., 2005. Provenance analysis by single-quartz-grain SEM-CL/optical microscopy. Journal of Sedimentary Research 75 (3), 492–500.

Bonnet, E., Bour, O., Odling, N.E., Davy, P., Main, I., Cowie, P., Berkowitz, B., 2001. Scaling of fracture systems in geological media. Reviews of Geophysics 39 (3), 347–383.

Clark, M.B., Brantley, S.L., Fisher, D.M., 1995. Power-law vein-thickness distributions and positive feedback in vein growth. Geology 23 (11), 975–978.

Dickinson, W.W., Milliken, K.L., 1995. The diagenetic role of brittle deformation in compaction and pressure solution of quartzose sandstones. Journal of Geology 103, 339–347.

Dutton, S.P., Clift, S.J., Hamilton, D.S., Hamlin, H.S., Hentz, T.F., Howard, W.E., Akhter, M.S., Laubach, S.E., 1993. Major low-permeability sandstone gas reservoirs in the Continental United States. The University of Texas at Austin, Bureau of Economic Geology Report of Investigations No. 211, 221 pp.

Gillespie, P.A., Walsh, J.J., Watterson, J., Bonson, C.G., Manzocchi, T., 2001. Scaling relationships of joint and vein arrays from The Burren, Co. Clare, Ireland. Journal of Structural Geology 23, 183–201.

Gomez, L.A., Laubach, S.E., 2006. Rapid digital quantification of microfracture populations. Journal of Structural Geology 28, 408–420.

Gomez, L.A., Gale, J.F.W., Laubach, S.E., Cumella, S., 2003. Chapter 6, Quantifying fracture intensity: an example from the Piceance basin. In: Peterson, K.M., Olson, T.M., Anderson, D.S. (Eds.), Piceance Basin 2003 Guidebook. Rocky Mountain Association of Geologists, pp. 96–113.

Griffith, A.A., 1920. The phenomena of rupture and flow in solids. Philosophical Transactions of the Royal Society of London A221, 163–198.

Gross, M.R., Engelder, T., 1995. Strain accommodated by brittle failure in adjacent units of the Monterey Formation, U.S.A.: scale effects and evidence for uniform displacement boundary conditions. Journal of Structural Geology 17 (9), 1303–1318.

Gudmundsson, A., 1987. Geometry, formation, and development of tectonic fractures on the Reykjanes Peninsula, southwest Iceland. Tectonophysics 139, 295–308.

Hansley, P.L., Johnson, R.C., 1980. Mineralogy and diagenesis of low-permeability sandstones of Late Cretaceous age, Piceance Creek basin, northwestern Colorado. The Mountain Geologist 17 (4), 88–129.

Hooker, J.N., Laubach, S.E., 2007. The geologic history of quartz grains, as revealed by color SEM-CL. Gulf Coast Association of Geological Societies Transactions 57, 375–386.

Johnson, R.C., Keighin, C.W., 1981. Cretaceous and Tertiary history and resources of the Piceance Creek basin, western Colorado. New Mexico Geological Society Guidebook, 32nd Field Conference, Western Slope Colorado.

Landtwing, M.R., Pettke, T., 2005. Relationships between SEM-cathodoluminescence response and trace-element composition of hydrothermal vein quartz. American Mineralogist 90, 122–131.

Laubach, S.E., 1997. A method to detect natural fracture strike in sandstones. Bulletin of the American Association of Petroleum Geologists 81 (4), 604–623.

Laubach, S.E., 2003. Practical approaches to identifying sealed and open fractures: Bulletin of the American Association of Petroleum Geologists 87 (4), 561–579.

Laubach, S.E., Diaz-Tushman, K., 2009. Laurentian paleostress trajectories and ephemeral fracture permeability, Cambrian Eriboll Formation sandstones west of the Moine thrust zone, northwest Scotland. Journal of the Geological Society (London) 166 (2), 345–360.

Laubach, S.E., Ward, M.E., 2006. Diagenesis in porosity evolution of opening-mode fractures, Middle Triassic to Lower Jurassic La Boca Formation, NE Mexico. Tectonophysics 419 (1–4), 75–97.

Lorenz, J.C., 1983. Lateral variability in the Corcoran and Cozzette blanket sandstones and associated Mesaverde rocks, Piceance Creek basin, northwestern Colorado. Society of Petroleum Engineers, SPE/DOE Paper 11608, 81-86.

Lorenz, J.C., Finley, S.J., 1991. Regional fractures II: fracturing of Mesaverde reservoirs in the Piceance basin, Colorado. Bulletin of the American Association of Petroleum Geologists 75 (11), 1738–1757.

Lorenz, J.C., Hill, R., 1991. Subsurface fracture spacing: comparison of inferences from slant/horizontal core and vertical core in Mesaverde reservoirs in the Piceance basin: SPE Rocky Mountain Regional Meeting and Low-Permeability Reservoir Symposium, April 15–17, Denver, SPE No. 21877, pp. 705-716.

Loriga, M.A., 1999. Scaling systematics of vein size: an example from the Guanajuato mining district (central Mexico). Geological Society of London Special Publications vol. 155, 57–67.

Mann, R.L., 1993. Slant hole completion test final report. Report DOE/MC/26024-3528 filed for the Department of Energy by CER Corporation, 87 pp.

Marrett, R., Ortega, O.J., Kelsey, C.M., 1999. Extent of power-law scaling for natural fractures in rock. Geology 27 (9), 799–802.

Nuccio, V.F., Condon, S.M., 1996. Burial and thermal history in the Paradox basin, Utah and Colorado, and petroleum potential of the Middle Pennsylvanian Paradox Formation. U.S. Geological Survey Bulletin 2000-O.

Nuccio, V.F., Roberts, L.N.R., 2003. Thermal maturity and oil and gas generation history of petroleum systems in the Uinta-Piceance Province, Utah and Colorado. In: Petroleum Systems and Geologic Assessment of Oil and Gas in the

Uinta-Piceance Province, Utah and Colorado. U.S. Geological Survey Digital Data Series DDS-69-B, Chapter 4.
Odling, N.E., 1997. Scaling and connectivity of joint systems in sandstones from western Norway. Journal of Structural Geology 19 (10), 1257–1271.
Odling, N.E., Gillespie, P., Bourgine, B., Castaing, C., Chiles, J.-P., Christensen, N.P., Fillion, E., Genter, A., Olsen, C., Thrane, L., Trice, R., Aarseth, E., Walsh, J.J., Watterson, J., 1999. Variations in fracture system geometry and their implications for fluid flow in fractured hydrocarbon reservoirs. Petroleum Geoscience 5, 373–384.
Ortega, O.J., Marrett, R., 2000. Prediction of macrofracture properties using microfracture information, Mesaverde Group sandstones, San Juan basin, New Mexico. Journal of Structural Geology 22 (5), 571–588.
Ortega, O., Marrett, R., Laubach, S.E., 2006. A scale-independent approach to fracture intensity and average spacing measurement. Bulletin of the American Association of Petroleum Geologists 90 (2), 193–208.
Pickering, G., Bull, J.M., Sanderson, D.J., 1995. Sampling power law distributions. Tectonophysics 248 (1–2), 1–20.
Quigley, M.D., 1965. Geologic history of Piceance Creek-Eagle basins. Bulletin of the American Association of Petroleum Geologists 49 (11), 1974–1996.
Reed, R.M., Milliken, K.L., 2003. How to overcome imaging problems associated with carbonate minerals on SEM-based cathodoluminescence systems. Journal of Sedimentary Research 73 (2), 328–332.
Renshaw, C.E., Pollard, D.D., 1995. An experimentally verified criterion for propagation across unbounded frictional interfaces in brittle, linear elastic materials. International Journal of Rock Mechanics and Mining Sciences and Geomechanics Abstracts 32, 237–249.
Rives, T., Razack, M.M., Petit, L.-R., Rawnsley, K.D., 1992. Joint spacing: analogue and numerical simulations. Journal of Structural Geology 14, 925–937.
Rusk, B., Reed, M., 2002. Scanning electron microscope-cathodoluminescence analysis of quartz reveals complex growth histories in veins from the Butte porphyry copper deposit, Montana. Geology 30 (8), 727–730.
Secor, D.T., 1965. Role of fluid pressure in jointing. American Journal of Science 263, 633–646.
Segall, P., 1984. Formation and growth of extensional fracture sets. Geological Society of America Bulletin 95 (4), 454–462.
Seyedolali, A., Krinsley, D.H., Boggs Jr., S., O'Hara, P.F., Dypvik, H., Goles, G.G., 1997. Provenance interpretation of quartz by scanning electron microscope-cathodoluminescence fabric analysis. Geology 25 (9), 787–790.
Sprunt, E.S., Nur, A., 1979. Microcracking and healing in granites: New evidence from cathodoluminescence. Science 205, 495–497.
Zapp, A.D., Cobban, W.A., 1960. Some Late Cretaceous strand lines in northwestern Colorado and northeastern Utah. U.S. Department of the Interior Short Papers in the Geological Sciences—Geological Survey Research 1960, U.S. Geological Survey Professional Paper 400-B, B246–249.